Check for updates

Effect of inorganic–organic surface modification of calcium sulfate whiskers on mechanical and thermal properties of calcium sulfate whisker/poly(vinyl chloride) composites

Yunhua Lu,[a] Nan Jiang,[b] Xingwei Li[a] and Shiai Xu [iD] *[ab]

Coupling agents are traditionally used to improve the interfacial adhesion between inorganic fillers and a polymer matrix; however, the application of this method is somewhat limited by the number of hydroxyl groups on the surface of inorganic fillers. In this study, a layer of calcium hydroxide ($Ca(OH)_2$) was coated on the surfaces of calcium sulfate whiskers (CSW) through hydroxylation modification using sodium hydroxide (NaOH) to increase the hydroxyl groups of the CSW, and then a polyether titanate coupling agent synthesized in our lab was used to modify $Ca(OH)_2$ coated CSW in order to improve their compatibility with poly(vinyl chloride) (PVC). The chemical structure and surface properties of the modified CSW were characterized by X-ray diffraction (XRD), Fourier transform infrared (FTIR) spectroscopy, scanning electron microscopy (SEM), energy dispersive spectroscopy (EDS), X-ray photoelectron spectroscopy (XPS) and water contact angle (WCA). Then, CSW/PVC and modified CSW/PVC composites were prepared *via* a two-roll mill, and the effects of the inorganic–organic surface modification of CSW on their mechanical and thermal properties were evaluated. The results show that hydroxylation modification can further improve the compatibility and the interfacial adhesion between CSW and the PVC matrix, which results in better mechanical and thermal properties.

1. Introduction

Calcium sulfate whiskers (CSW) are one of the most promising reinforcing fillers capable of improving the performance (*e.g.*, impact resistance, Young's modulus and thermal resistance) of poly(vinyl chloride) PVC composites[1–5] due to their outstanding properties such as integrated shape, high intensity, high-temperature resistance, large aspect ratio and high tenacity.[6,7] However, because of their high surface energy, CSWs incorporated in the polymer matrix are prone to aggregation and hence often exhibit poor dispersion, which can compromise the performance of the composites.[8] In addition, the distinct difference in the surface energy between hydrophilic CSW and hydrophobic polymers is the main contributor to the poor interfacial interaction.[9] Thus, many efforts have been devoted to convert the hydrophilic surface into a hydrophobic one to improve the compatibility between CSW and the polymer matrix.[1,10–12] Surface modification is able to improve the interfacial affinity between the inorganic fillers and the polymer matrix.[13–21] This is typically accomplished with the use of

coupling agents capable of reacting with hydroxyl groups. Ma *et al.*[22] used a KH570 silane coupling agent to improve the dispersion stability of ZnO nanoparticles. Truong *et al.*[23] treated Al_2O_3 nanoparticle surface with two different silane coupling agents to improve hydrophobic interactions with the syndiotactic polypropylene matrix. Yang *et al.*[24] modified nano-$CaCO_3$ using three different coupling agents (KH560, KH570 and NDZ-101) and then prepared silicone rubber/nano-$CaCO_3$ shell–core structured fillers to reinforce rigid PVC. Shah *et al.*[25] have shown that chitin and chitosan as novel coupling agents could effectively improve the interfacial adhesion between the wood fibers and PVC. However, the surface modification effect of these coupling agents depends heavily on the hydroxyl number on the surface of the fillers, and rather disappointingly, it is not desirable in most cases because of the small number of hydroxyl groups on the surface of most inorganic fillers. Obviously, it is important to increase the number of hydroxyl groups on the surface of some inorganic fillers. In our previous work, a polyether titanate coupling agent (eTi_{4000}) synthesized using polyethyleneglycol (PEG4000) was directly used to modify the surface of CSW.[26] The hydroxyl groups on the CSW surface can interact with eTi_{4000} to bridge CSW and PVC matrix, but the modification effect is also restricted by the limited number of hydroxyl groups on the CSW surface, thus affecting the overall performance of the PVC composites.

[a] *Key Laboratory for Ultrafine Materials of Ministry of Education, School of Materials Science and Engineering, East China University of Science and Technology, Shanghai 200237, China. E-mail: saxu@ecust.edu.cn; Tel: +86-021-64253353*
[b] *School of Chemical Engineering, Qinghai University, Xining 810016, China*

In this study, a layer of calcium hydroxide ($Ca(OH)_2$) was coated on the surface of CSW by a simple precipitation reaction in order to impart CSW surface with more hydroxyl groups, which was then treated with a polyether titanate coupling agent (eTi_{4000}) synthesized in our lab in order to further improve the interfacial adhesion strength between CSW and the PVC matrix. The chemical structure and surface properties of modified CSW (mCSW) were characterized by X-ray diffraction (XRD), Fourier transform infrared (FTIR) spectroscopy, scanning electron microscopy (SEM), energy dispersive spectroscopy (EDS), X-ray photoelectron spectroscopy (XPS) and water contact angle (WCA), and the effect of inorganic–organic surface modification of CSW on the mechanical and thermal properties of PVC composites was evaluated.

2. Experimental

2.1. Materials

Sodium hydrate (analytically pure) and anhydrous sodium sulfate (analytically pure) were purchased from Shanghai Lingfeng Reagent Co., Ltd. (Shanghai, China). PVC (SG-5) (particle size: 200–250 μm; intrinsic viscosity: 112 mL g^{-1}; the number of impurity ions ≤ 10; the volatile matter content ≤ 0.16%; apparent density ≥ 0.54 g mL^{-1}; whiteness% ≥ 84.1) was purchased from Dongguan Dansheng Plastic Materials Co., Ltd., (Dongguan, China). CSWs (average diameter: 1–8 μm; average length: 30–200 μm; melting point: 1450 °C; whiteness% ≥ 98; density: 2.69 g cm^{-3}; pH: 6–8; water solubility ≤ 1200 ppm (22 °C)) were purchased from Shanghai Fengzhu Trading Co., Ltd. (Shanghai, China). Organic tin, dioctyl phthalate (DOP), glyceryl monosterate (GMS), acrylic processing aid (ACR) and paraffin wax were commercially available and all of them were of technical grade.

2.2. Modification of CSW

mCSW with rich hydroxyl groups (OH-CSW) were prepared as follows: 40 g of NaOH and 14.2 g of Na_2SO_4 were added into 1 L of distilled water in a three-necked round-bottom flask fitted with a mechanical overhead stirrer. Then, 542.0 g of CSW was added into the solution and vigorously stirred at 25 °C in water bath for 2 h. The slurry was filtered, washed with distilled water until the pH was around 7 and dried at 100 °C for 24 h. OH-CSW was modified by eTi_{4000} as follows: 3 wt% coupling agent eTi_{4000} relative to OH-CSW was pre-hydrolyzed in 95 wt% ethanol solution, and then a certain amount of OH-CSW was sequentially added into a three-necked round-bottom flask fitted with a mechanical overhead stirrer. The mixture was stirred at 75 °C for 4 h, and the obtained products were dried under vacuum at 100 °C for 2 h to remove excess water and the inorganic–organic modified CSW (eTi_{4000}-OH-CSW) was prepared.

2.3. Preparation of PVC composites

The PVC composites were prepared as described in our previous study:[26] PVC resin (100 phr) was mixed with various contents of CSW or mCSW (including eTi_{4000}-CSW and eTi_{4000}-OH-CSW) using organic tin (2 phr) as a heat stabilizer and DOP (4 phr)

as a plasticizer. GMS (0.6 phr), ACR (4 phr), and paraffin wax (0.4 phr) were then added. The mixture was mixed thoroughly and then processed using a two-roll mill at 170 °C for 10 min (nip gap: 1 mm, rotating speed: 20 rpm). The resultant compound was molded into rectangular sheets by compression molding at 170 °C and 10 MPa for 5 min using a plate vulcanizing press. As a control, PVC without whisker was prepared following to the same procedure.

2.4. Characterization and measurements

The FTIR spectra were recorded on a Nicolet 6700 FT-IR spectrometer (New York, USA) with a scan number of 32 and a resolution of 4 cm^{-1}. XRD patterns were determined on D/Max 2550v diffractometer (Tokyo, Japan) using Cu Kα radiation. The surface morphology was characterized by XPS (ESCALAB 250Xi, New York, USA) with a Mg Kα photon energy of 1253.6 eV. WCA (JC2000D1, Shanghai, China) was measured to determine the hydrophobicity of samples. Drops of deionized water (3 μL) were deposited on six different spots of each surface, and the average of the six measurements was reported. The tensile and flexural properties were determined using a MTS E44 universal testing machine in accordance with ISO 527 and ISO 178, respectively. At least five independent measurements were made for each sample. The dynamic mechanical properties were determined using a TA Instruments Q800 (TA instruments, New Castle, USA) in a three-point bending mode at a vibration frequency of 1 Hz from 25 to 140 °C at a heating rate of 3 °C min^{-1}. The cryo-fractured surfaces in liquid nitrogen and the tensile fractured surfaces of the samples were observed using a S-4800 field emission scanning electron microscope (SEM, Tokyo, Japan). Prior to SEM observation, the fracture surfaces were coated with a thin gold layer. Vicat softening temperatures (VST) were measured using a VST tester (ZWK1302-B, MTS, Shenzhen, China) in accordance with ISO 306 at a load of 10 N and a heating rate of 120 °C h^{-1}. Thermogravimetric analysis (TGA) was carried out using a Netzsch STA 409PC thermogravimetric analyzer at a heating rate of 10 °C min^{-1} to 600 °C under a nitrogen atmosphere.

3. Results and discussion

3.1. XRD and FTIR analysis

Fig. 1 shows the XRD patterns of CSW (Fig. 1a) and OH-CSW (Fig. 1b). Compared with Fig. 1a, new peaks are observed in Fig. 1b compared with Fig. 1a, which are assigned to the diffraction peaks of $Ca(OH)_2$ corresponding to the crystal faces of (101), (102) and (110). Also, Fig. 1b shows that the intensity of the diffraction peaks of CSW is weaker than that in Fig. 1a due to the presence of the $Ca(OH)_2$ layer coated on its surface.

Fig. 2 shows the FTIR spectra of CSW (Fig. 2a), OH-CSW (Fig. 2b), eTi_{4000}-CSW (Fig. 2c) and eTi_{4000}-OH-CSW (Fig. 2d). A weak absorption band is observed at around 3620 cm^{-1} in Fig. 2a, indicating that there are only a few hydroxyl groups on the surface of unmodified CSW. In Fig. 2b, the peak corresponding to the hydroxyl groups becomes much stronger, indicating that hydroxylation modification results in an increase in the number of hydroxyl groups on the surface of OH-
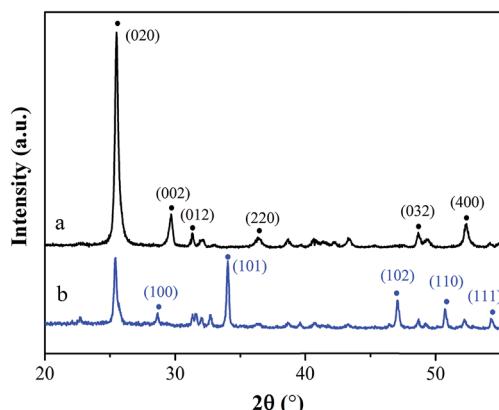
Fig. 1 XRD patterns of (a) CSW and (b) OH-CSW.
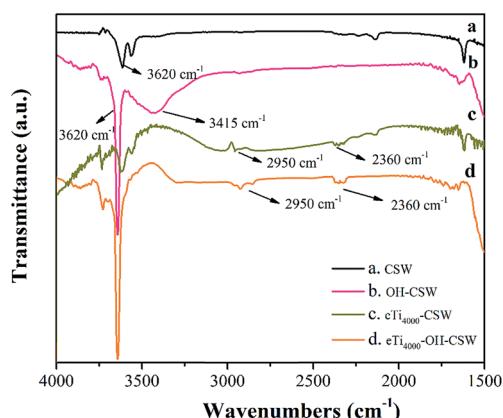
Fig. 2 FTIR spectra of (a) CSW, (b) OH-CSW, (c) eTi$_{4000}$-CSW and (d) eTi$_{4000}$-OH-CSW.

CSW. The broad absorption band at about 3415 cm^{-1} should be assigned to the stretching vibration of O–H groups that form hydrogen bond. Compared with CSW, two new absorption peaks are observed at 2950 cm^{-1} and 2360 cm^{-1} in the FTIR spectra of eTi$_{4000}$-CSW and eTi$_{4000}$-OH-CSW, which are the characteristic absorption bands of eTi$_{4000}$. Thus, CSW has been successfully modified by eTi$_{4000}$.

3.2.   XPS and WCA measurement

The XPS spectra of CSW, eTi$_{4000}$-CSW, OH-CSW and eTi$_{4000}$-OH-CSW are shown in Fig. 3a, b, c and d, respectively, and Fig. 3a and b are taken from our previous work.[26] In the O 1s XPS spectra (Fig. 3a), the peak at 532.0 eV is attributed to the interaction between Ca^{2+} and SO$_4^{2-}$, and the signal of C–O at 532.6 eV might be due to the impurity or contamination. The peak at 531.7 eV in Fig. 3b is attributed to the O–H bond resulting from the crystal water in the modification process and the coupling agent with hydroxyl groups. The peak at 532.6 eV is assigned to C–O. However, the peak at 532.6 eV in Fig. 3b is larger than that in Fig. 3a, indicating successful modification by eTi$_{4000}$. The comparison between Fig. 3a and c shows that the peak at 531.2 eV is attributed to the Ca(OH)$_2$ layer coated on CSW surface due to the partial substitution of SO$_4^{2-}$ by OH$^-$.

The peak at 531.2 eV in Fig. 3d becomes weaker than that in Fig. 3c, this is because some hydroxyl groups are depleted by the coupling reaction with eTi$_{4000}$. The peak at 532.6 eV in Fig. 3d is marginally larger than that in Fig, 3c, indicating that more eTi$_{4000}$ has been grafted on CSW surface after the hydroxylation modification. These results are consistent with FTIR spectra.

The surface properties of CSW and mCSW are evaluated by WCA, which gives the information of affinity between CSW and the PVC matrix. Fig. 4 shows the WCA on CSW, eTi$_{4000}$-CSW, OH-CSW and eTi$_{4000}$-OH-CSW, respectively. The WCA of CSW is 24.5°, indicating poor hydrophobicity, while that of eTi$_{4000}$-CSW is increased to 78.5°, indicating that modification by eTi$_{4000}$ enable the CSW surface to be more hydrophobic. However, it is interesting to note that the WCA of OH-CSW is reduced to 18.0° (Fig. 4c) showing an increase in hydrophilicity compared with CSW (Fig. 4a), which can be attributed to the Ca(OH)$_2$ layer coated on the CSW surface. Furthermore, the WCA of eTi$_{4000}$-OH-CSW is 89.4°, indicating that its hydrophobicity is further increased compared with eTi$_{4000}$-CSW. The results indicate that the chemical reactivity of CSW is enhanced after hydroxylation, because the Ca(OH)$_2$ layer coated on the CSW surface can provide more hydroxyl groups which can react with more eTi$_{4000}$ molecules compared with untreated CSW. Thus, the more the coupling agent eTi$_{4000}$ bonded on the OH-CSW surface, the better the hydrophobicity of eTi$_{4000}$-OH-CSW and the compatibility between CSW and the PVC matrix will be.

3.3.   SEM analysis

The SEM images of CSW, eTi$_{4000}$-CSW, OH-CSW and eTi$_{4000}$-OH-CSW are shown in Fig. 5, and the insert at the top right corner shows the enlarged images of samples in order to observe the fine structure of whisker surface more clearly. Fig. 5A and B clearly show that modification by eTi$_{4000}$ results in no significant changes in the surface morphology of eTi$_{4000}$-CSW, indicating that the morphology can be hardly affected by eTi$_{4000}$ modification. However, NaOH hydroxylation makes the CSW surface rougher due to the deposition of Ca(OH)$_2$ layer (Fig. 5C). And Fig. 5D shows that the surface morphology of eTi$_{4000}$-OH-CSW is similar to that of OH-CSW. The deposition process of Ca(OH)$_2$ is assumed to occur on the surface of CSW when NaOH and Na$_2$SO$_4$ are added into the suspension. There is a chemical equilibrium in the solution:

$$CaSO_4 + 2NaOH \rightleftharpoons Na_2SO_4 + Ca(OH)_2$$
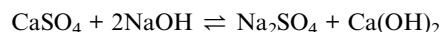
The chemical structure of eTi$_{4000}$ is presented in Scheme 1. The corresponding EDS spectra of CSW, eTi$_{4000}$-CSW, OH-CSW and eTi$_{4000}$-OH-CSW are shown in Fig. 5a, b, c and d, respectively, and the EDS results are summarized in Table 1. The EDS results of CSW and eTi$_{4000}$-CSW are taken from our previous study for comparison.[26] The comparison between CSW and eTi$_{4000}$-CSW shows that eTi$_{4000}$ modification should be responsible for the increase of O content and the decrease of Ca and S content in eTi$_{4000}$-CSW. A significant amount of P and Ti elements are also detected on the eTi$_{4000}$-CSW surfaces. However, for OH-CSW, the Ca(OH)$_2$ layer leads to an increase in the O and Ca content as well as a decrease in the S content. For
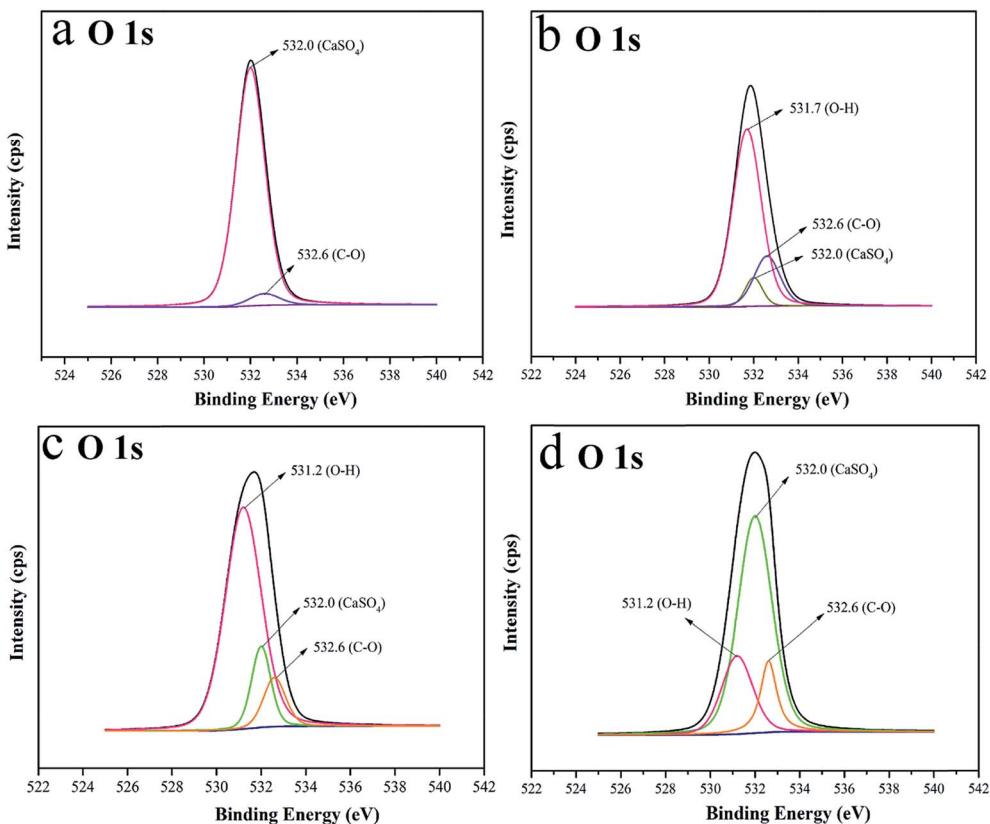
Fig. 3 XPS high-resolution spectra of the O 1s region of (a) CSW; (b) eTi_{4000}-CSW, (c) OH-CSW, and (d) eTi_{4000}-OH-CSW.
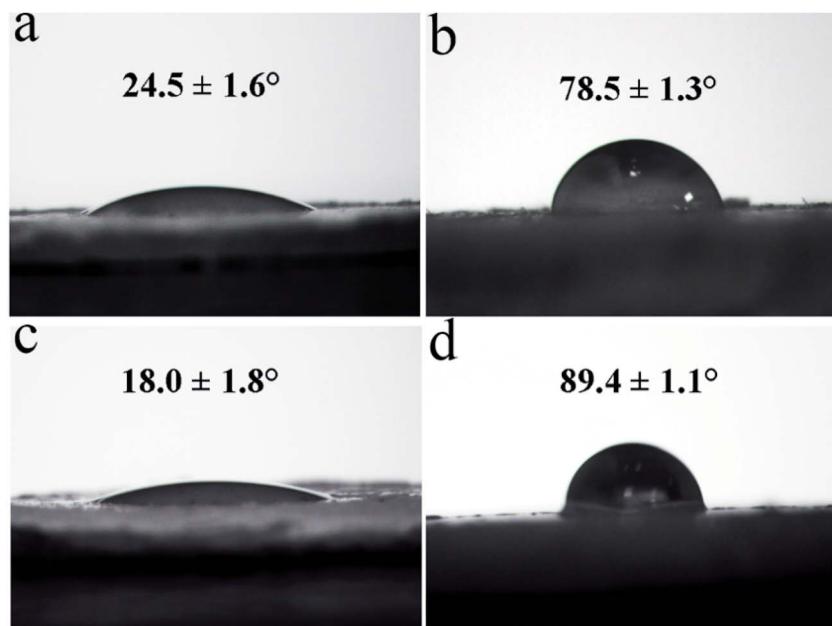
Fig. 4 WCAs on (a) CSW, (b) eTi_{4000}-CSW, (c) OH-CSW, and (d) eTi_{4000}-OH-CSW.

eTi_{4000}-OH-CSW, the P and Ti content increases to different extents compared with eTi_{4000}-CSW, indicating that after hydroxylation, the more the hydroxyl groups on the CSW surface, the more the eTi_{4000} can be bonded.

3.4. Mechanical performance of PVC composites

The tensile properties of pure PVC, CSW/PVC, eTi_{4000}-CSW/PVC and eTi_{4000}-OH-CSW/PVC composites, as a function of filler loading (0 to 30 wt%) are shown in Fig. 6. Fig. 6a shows that the
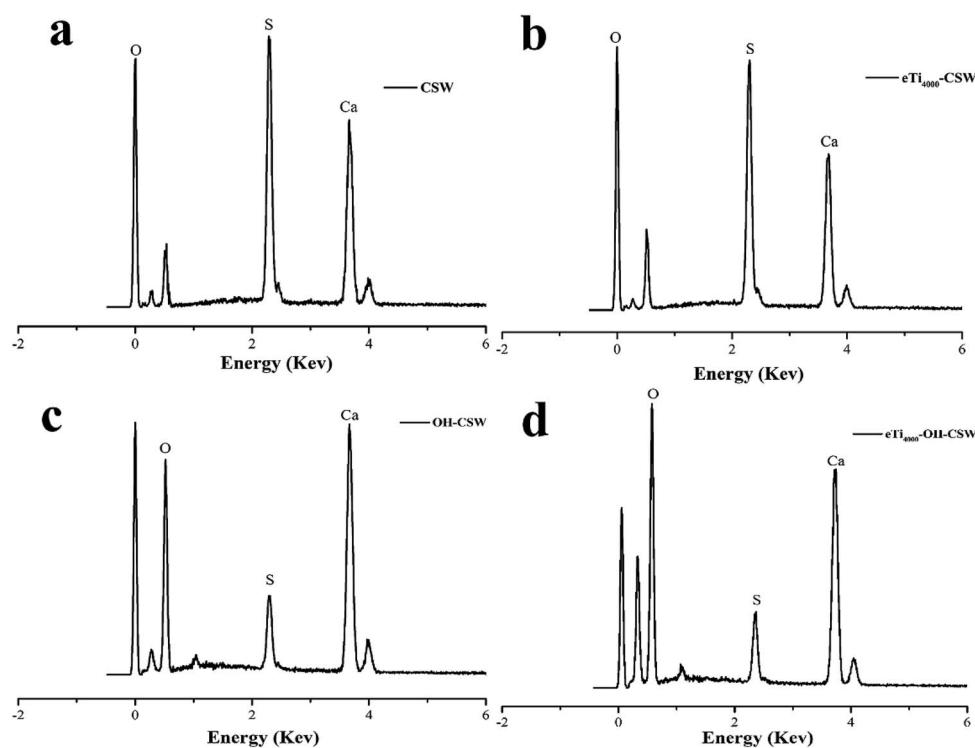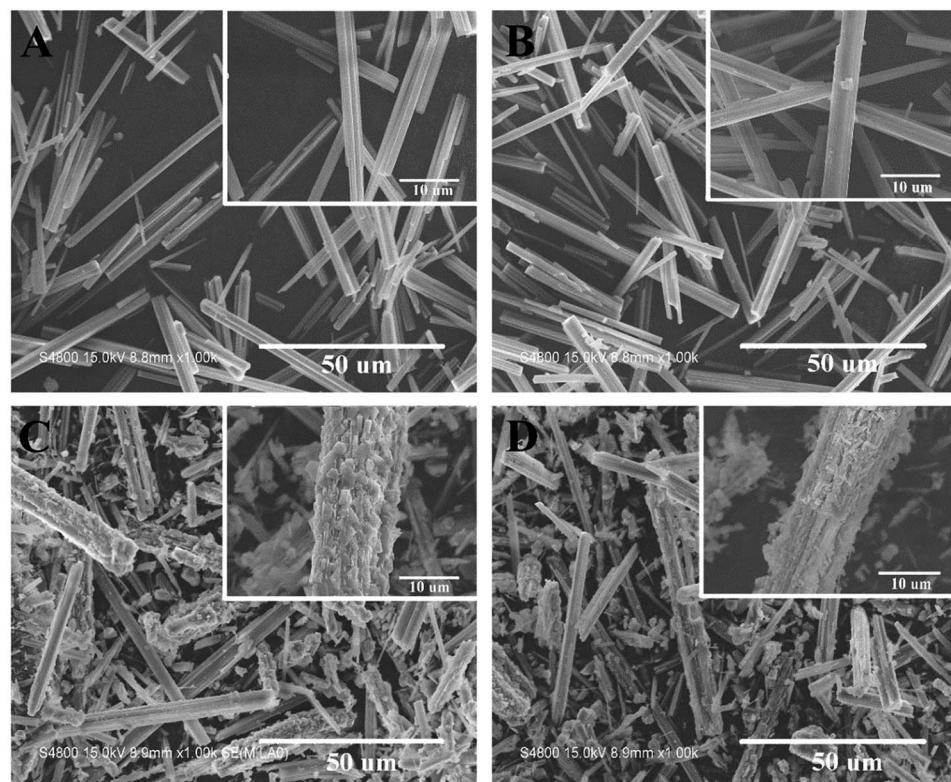
Fig. 5 SEM images and EDS spectra of (A, a) CSW; (B, b) eTi_{4000}-CSW; (C, c) OH-CSW; and (D, d) eTi_{4000}-OH-CSW.

Young's modulus of all composites is much higher than that of the PVC matrix, indicating that the addition of CSW, unmodified and modified alike, can increase the stiffness of the PVC

matrix. The Young's modulus is the ratio of stress to strain in the elastic range. However, as the strain in elastic deformation is very small for polymer composites, the Young's modulus is
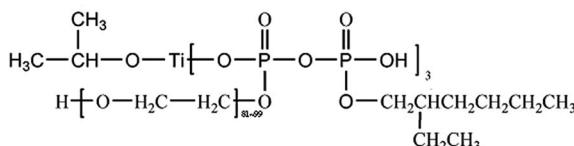
Scheme 1 The chemical structure of eTi$_{4000}$.

not so sensitive to the interfacial adhesion. As CSW has a much higher Young's modulus than the PVC matrix, the Young's modulus of the composites tends to increase with the increase of CSW loading.[27] In addition, eTi$_{4000}$-CSW/PVC and eTi$_{4000}$-OH-CSW/PVC composites have a higher Young's modulus than CSW/PVC composites, indicating that surface modification can further improve the reinforcement effect of CSW.

The yield strength, breaking strength and elongation at break are much more sensitive than Young's modulus to the

interfacial adhesion, because these parameters are more intimately associated with plastic deformation. It is shown that the yield strength of CSW/PVC composites is lower than that of the PVC matrix, and it decreases sharply with the increase of CSW content (Fig. 6b). A similar trend can also be observed for eTi$_{4000}$-CSW/PVC composites, although they have a higher yield strength than those CSW/PVC composites with the same CSW content. It is interesting that the yield strength of eTi$_{4000}$-OH-CSW/PVC composites has a relatively low dependence on CSW content, and it is much higher than that of CSW/PVC and eTi$_{4000}$-CSW/PVC composites, especially at high CSW loadings. For example, the yield strength of the eTi$_{4000}$-OH-CSW/PVC composite with 30 wt% of CSW is 53.8 MPa, which is much higher than that of CSW/PVC (35.6 MPa) and eTi$_{4000}$-CSW/PVC (40.8 MPa) composites with the same CSW loading.

Fig. 6c shows that surface treatment also plays a key role in the breaking strength of the composites. eTi$_{4000}$-OH-CSW/PVC

Table 1 The EDS results of CSW, eTi$_{4000}$-CSW, OH-CSW and eTi$_{4000}$-OH-CSW

| Sample	CSW		eTi$_{4000}$-CSW		OH-CSW		eTi$_{4000}$-OH-CSW	
	Weight (wt%)	Atom (at%)	Weight (wt%)	Atom (at%)	Weight (wt%)	Atom (at%)	Weight (wt%)	Atom (at%)
O	44.70 ± 12.30	59.50 ± 11.50	54.32 ± 8.00	66.51 ± 8.80	54.10 ± 7.80	66.70 ± 2.40	61.88 ± 11.20	65.24 ± 3.90
Ca	30.60 ± 5.20	20.20 ± 2.20	25.43 ± 2.50	15.73 ± 2.30	39.10 ± 7.60	27.10 ± 5.40	33.22 ± 7.40	27.90 ± 4.50
S	24.70 ± 1.60	20.30 ± 2.50	20.02 ± 1.40	17.67 ± 1.20	6.80 ± 0.80	6.20 ± 0.10	4.00 ± 0.20	6.60 ± 0.20
P	0	0	0.19 ± 0.01	0.07 ± 0.03	0	0	0.48 ± 0.40	0.21 ± 0.09
Ti	0	0	0.04 ± 0.01	0.02 ± 0.00	0	0	0.10 ± 0.02	0.05 ± 0.02
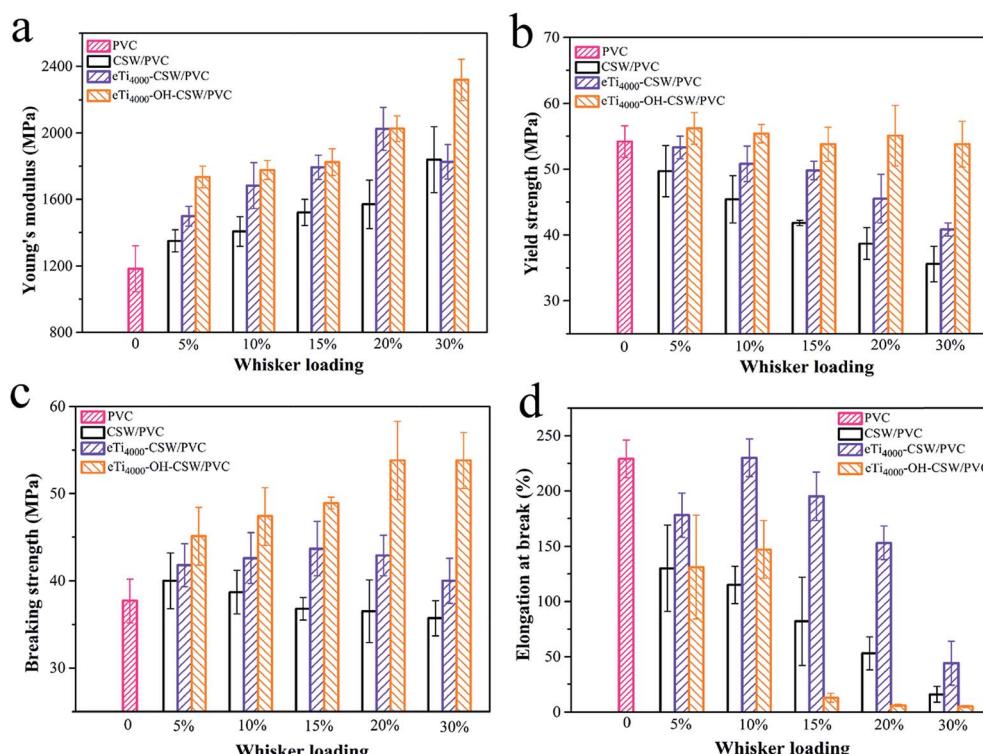
Fig. 6 Tensile properties of CSW/PVC and mCSW/PVC composites with various whisker contents: (a) Yong's modulus; (b) yield strength; (c) breaking strength; and (d) elongation at break.
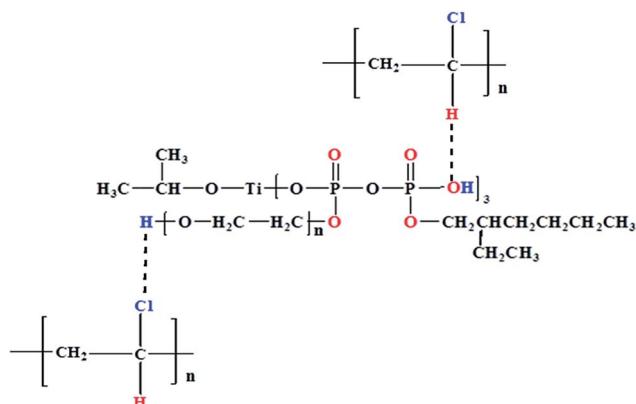
Fig. 7 The hydrogen bonds between PVC and titanate.

composites have the highest breaking strength at the same CSW loading owing to the strongest interfacial adhesion between eTi$_{4000}$-OH-CSW and the matrix. For unmodified CSW/PVC composites, the poor compatibility between CSW and the PVC matrix leads to poor stress transfer at the filler/matrix interface,[28–30] and consequently poor mechanical properties of CSW/PVC composites.

The elongation at break of eTi$_{4000}$-OH-CSW/PVC composites first increases with increasing CSW loading and reaches a maximum of 147% at 10 wt% of CSW, with an increase of 28% compared with unmodified CSW/PVC composites. However, it shows a substantial decrease with further increase of CSW loading, which is characteristic of brittle fracture. These results can be explained by the following reasons. First, it is known that stress concentration plays an important role in initiating plastic deformation of the polymer matrix, such as crazing or shearing.[31] Due to the strong interfacial adhesion between eTi$_{4000}$-OH-CSW and the PVC matrix, the stress can be effectively transferred between them. Thus, debonding is unlikely to occur between CSW and the matrix, and the stress concentration effect of CSW is highly limited and cannot initiate sufficient plastic deformation of the matrix, resulting in an abrupt decrease in elongation at break at high CSW loadings. On the

other hand, the fibrillar whisker can restrict the polymer chain motion of the matrix,[32] which is greatly enhanced by the strong interfacial adhesion.

The strong interfacial adhesion of the composites originates from the interaction between the two phases. Because both PVC and titanate are polar molecules, there are electrostatic interactions between them, which can contribute to the increase of the compatibility between CSW and PVC. On the other hand, the active hydrogen atom (marked red in the PVC structure in Fig. 7) is likely to form a weak hydrogen bond with oxygen atom (marked red in the titanate in Fig. 7).[33,34] Also, the chlorine atom (marked blue in the PVC structure in Fig. 7) can also form a weak hydrogen bond with hydrogen atom (marked blue in the titanate in Fig. 7). These hydrogen bonds contribute to improving the affinity between PVC and titanate. Thus, coupling agent molecules bonded on CSW surface can result in good interfacial compatibility and strong interfacial adhesion between CSW and the PVC matrix, and consequently an increase in strength and modulus.[28,29,35] After Ca(OH)$_2$ is deposited on the CSW surface, the number of hydroxyl groups on the CSW surface sharply increases, thus more titanate molecules can be linked on the CSW surface by chemical bonding, as shown in Fig. 8. As a result, the compatibility and the interfacial adhesion between CSW and the PVC matrix can be further improved by hydroxylation modification. The stress transfer is improved and the stress concentration effect at the CSW/PVC interface is minimized, resulting in higher Young's modulus, yield strength and breaking strength of eTi$_{4000}$-OH-CSW/PVC composites than CSW/PVC and eTi$_{4000}$-CSW/PVC composites at the same CSW loading.

The flexural modulus of PVC, CSW/PVC, eTi$_{4000}$-CSW/PVC and eTi$_{4000}$-OH-CSW/PVC composites is shown in Fig. 9. The flexural modulus of CSW/PVC composites increases with the increase of CSW loading in the PVC matrix. Titanate treatment leads to a further increase in flexural modulus of eTi$_{4000}$-CSW/PVC composites compared with that of unmodified CSW/PVC composites, which can be attributed to the improved interfacial compatibility. eTi$_{4000}$-OH-CSW/PVC composites exhibit an even higher flexural modulus than eTi$_{4000}$-CSW/PVC, especially
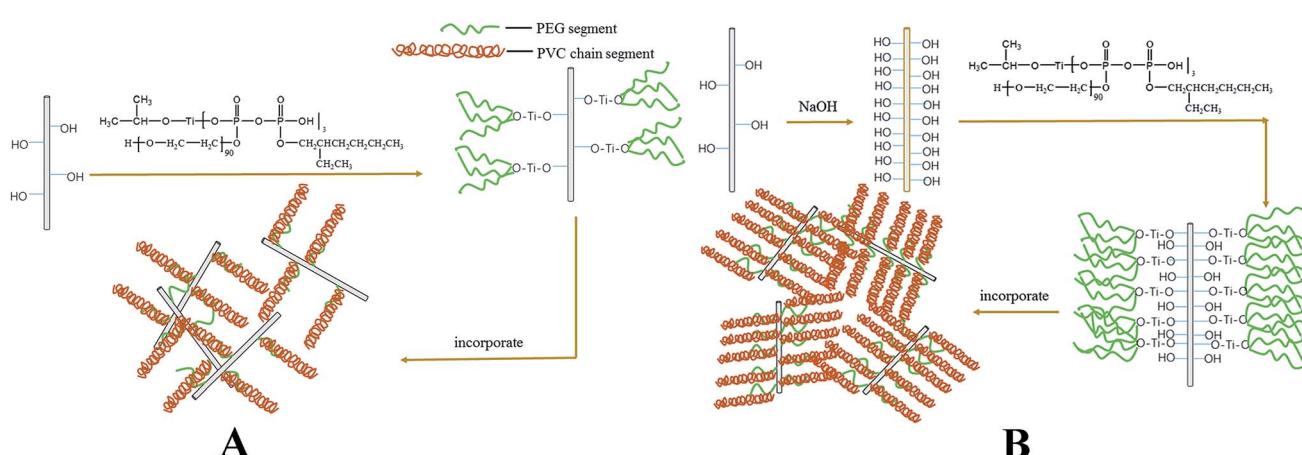
**Fig. 8** CSW modified by coupling agent and the interfacial interaction between CSW and PVC matrix.
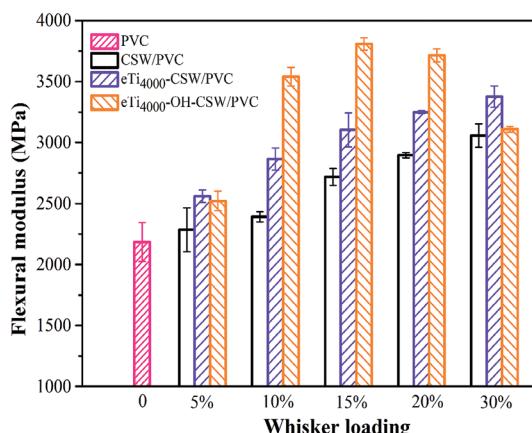
Fig. 9 Flexural properties of CSW/PVC and mCSW/PVC composites with various whisker contents.

at CSW loadings between 10–20 wt% due to the more homogeneous dispersion of eTi$_{4000}$-OH-CSW and the stronger adhesion between eTi$_{4000}$-OH-CSW and the PVC matrix. The flexural modulus of eTi$_{4000}$-OH-CSW/PVC composites with 15 wt% eTi$_{4000}$-OH-CSW reaches 3807 MPa, with an increase of 40% and 23% compared with that CSW/PVC and eTi$_{4000}$-CSW/PVC composites, respectively.

DMA test was performed to evaluate the effect of modification on the interfacial properties of composites under dynamic loading. The variations of the storage modulus (E') and tangent δ (tan δ) with temperature for CSW/PVC and mCSW/PVC

composites are shown in Fig. 10, and the storage modulus at 30 °C and the glass transition temperature determined from tan δ peak value of all composites are summarized in Tables 2 and 3 respectively. It can be seen from Table 2 that the storage modulus of unmodified CSW/PVC composites increases with the increase of CSW content until a maximum is reached at 15 wt%, after which it remains almost unchanged with further increase of CSW content. However, a quite different trend is observed for mCSW/PVC composites, and their storage modulus increases continually with the increase of mCSW content and it is higher than the corresponding CSW/PVC composite with the same CSW content. It is noteworthy that eTi$_{4000}$-OH-CSW/PVC composite even has a higher modulus compared with eTi$_{4000}$-CSW/PVC composite. This results indicate that the modification of CSW results in an increase in interfacial interaction, as described earlier.

It is interesting that the glass transition temperatures of all composites increase with CSW content at first and then decrease, and the maximum is reached at 20 wt% CSW for CSW/PVC composites, and at 15 wt% for mCSW/PVC composites, respectively (Table 3). Ou et al.[36] observed the similar trend in SiO$_2$/PMMA composite, which could be attributed to two inverse effects with the addition of inorganic fillers: (1) addition of inorganic fillers can restrict the motion of polymer chains, resulting in an increase in glass transition temperature with the filler content; (2) the addition of inorganic fillers can increase the free volume of composites, resulting in an increase in the motion of polymer chains, and consequently a decrease in glass transition temperature with the filler content. On the other
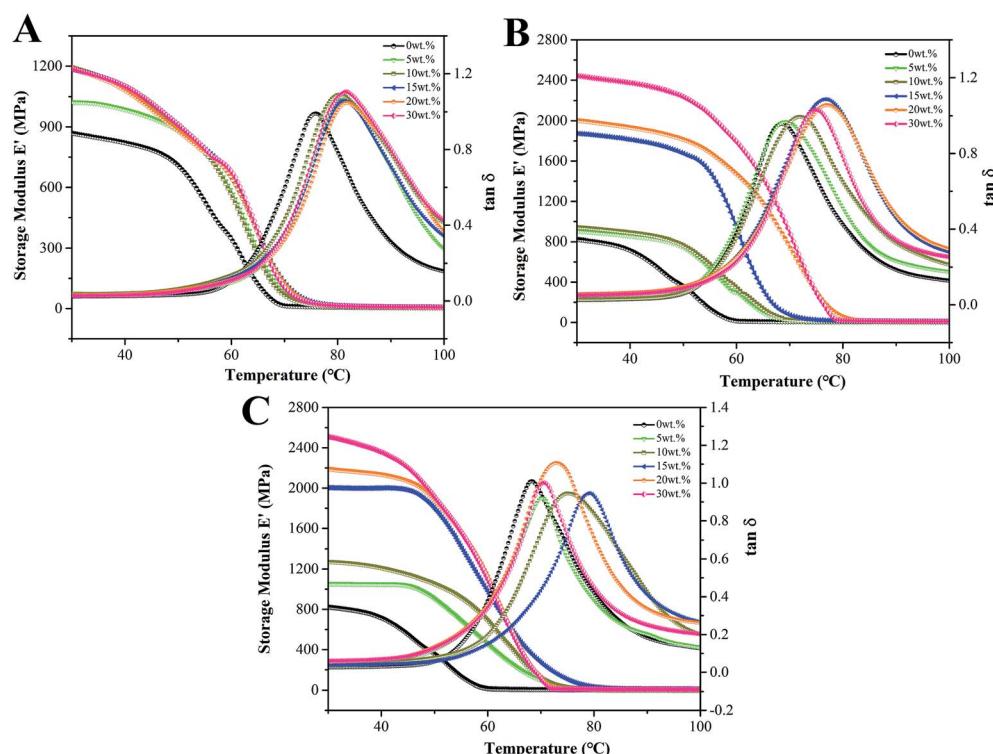

Fig. 10 DMA curves for CSW/PVC and mCSW/PVC composites with various whisker contents: (A) unmodified CSW/PVC, (B) eTi$_{4000}$-CSW/PVC and (C) eTi$_{4000}$-OH-CSW/PVC.

Table 2 The storage modulus of CSW/PVC and mCSW/PVC composites at 30 °C (MPa)

Whisker content (%)	0	5	10	15	20	30
CSW/PVC	869	914	957	1184	1189	1186
eTi_{4000}-CSW/PVC	869	1023	1194	1872	2033	2462
eTi_{4000}-OH-CSW/PVC	869	1064	1253	2018	2250	2517

Table 3 Glass transition temperature of CSW/PVC and mCSW/PVC composites

Whisker content (%)	0	5	10	15	20	30
CSW/PVC	68.2	69.5	72.0	74.2	75.1	74.7
eTi_{4000}-CSW/PVC	68.2	70.5	73.4	76.8	76.4	75.1
eTi_{4000}-OH-CSW/PVC	68.2	73.9	75.3	79.4	73.3	71.2

hand, because eTi_{4000} with long flexible segments can penetrate into the PVC matrix, the presence of eTi_{4000} segment can reduce to some extent the dipole–dipole interaction between PVC molecular chains. The molar fraction of eTi_{4000} segment increases with the content of mCSW, which makes the maximum glass transition temperature of mCSW/PVC earlier than that of unmodified CSW/PVC composite.

3.5. Morphology

SEM observation provides necessary information concerning the interfacial adhesion. Fig. 11 shows SEM images of the tensile fracture surfaces of CSW/PVC, eTi_{4000}-CSW/PVC and eTi_{4000}-OH-CSW/PVC composites with different whisker contents. The voids resulting from the pulling out of CSW from the matrix can be

readily seen in Fig. 11A1, because the large difference in polarity between CSW and PVC causes very poor interfacial compatibility. The CSW surface is relatively clean and smooth, indicating weak interactions between CSW and the matrix.[37,38] This is especially true at high CSW loadings (Fig. 11B1). The modification by eTi_{4000} results in an improvement of the interfacial compatibility between eTi_{4000}-CSW and the PVC matrix, and consequently intimate contact between them (Fig. 11A2). For eTi_{4000}-OH-CSW/PVC composites (Fig. 11A3), there is no obvious gap between CSW and the matrix, indicating that inorganic–organic modification results in a significant improvement of the interfacial adhesion. Importantly, many CSWs are broken in the tensile process, indicating that the applied stress can be efficiently transferred between the two phases.

The difference in interfacial adhesion between different composites becomes more pronounced at high CSW loadings (Fig. 11B1–B3). For CSW/PVC composite (Fig. 11B1), many intact CSWs with a smooth surface can be observed on the fracture surface (shown by arrows), indicating that the applied stress cannot be sufficiently transferred from the matrix to CSWs due to the poor interfacial adhesion. For eTi_{4000}-CSW/PVC composite, some broken CSWs (shown by arrows), as well as some intact CSWs, are observed. In contrast, for eTi_{4000}-OH-CSW/PVC composite, there are almost no intact CSWs on the surface, and they are fractured in the tensile process due to the applied stress transferred from the matrix, indicating strong interfacial adhesion between the two phases.

Fig. 12 shows SEM images of the cryo-fractured surfaces of CSW/PVC, eTi_{4000}-CSW/PVC and eTi_{4000}-OH-CSW/PVC composites with 5 wt% and 30 wt% CSW after quenching in liquid nitrogen, respectively. In Fig. 12A1, there are some smooth CSWs (shown by arrows) on the fractured surface, indicating pulling-out
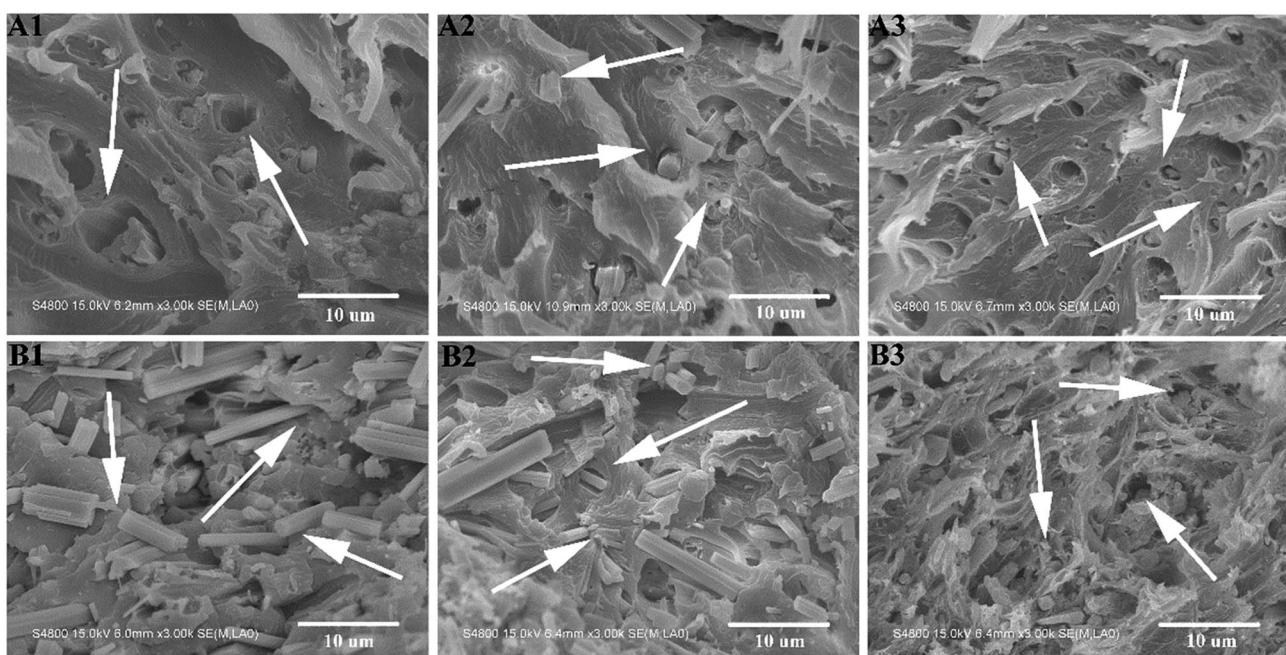
Fig. 11 SEM images of tensile fracture surfaces for the composites with 5 wt% whisker (A1 CSW/PVC, A2 eTi_{4000}-CSW/PVC and A3 eTi_{4000}-OH-CSW/PVC) and the composites with 30 wt% whisker (B1 CSW/PVC, B2 eTi_{4000}-CSW/PVC and B3 eTi_{4000}-OH-CSW/PVC).
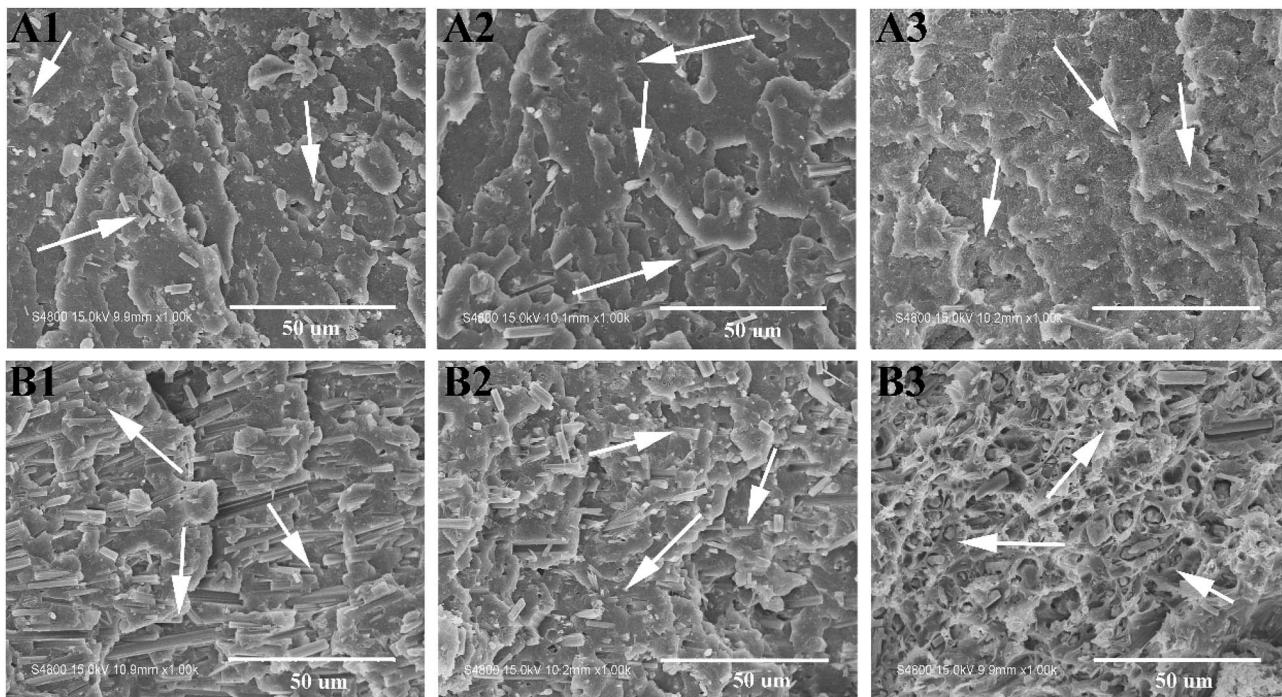
Fig. 12 SEM images of fracture surfaces for the composites with 5 wt% whisker (A1-CSW/PVC, A2-eTi$_{4000}$-CSW/PVC and A3-eTi$_{4000}$-OH-CSW/PVC) and the composites with 30 wt% whisker (B1-CSW/PVC, B2-eTi$_{4000}$-CSW/PVC and B3-eTi$_{4000}$-OH-CSW/PVC).
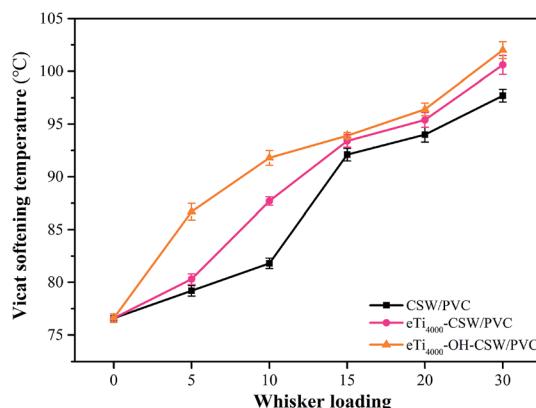
Fig. 13 VST of CSW/PVC and modified CSW/PVC composites with various filler contents.

More importantly, eTi$_{4000}$-OH-CSW are distributed homogeneously in the PVC matrix and no pulling-out of CSW from the matrix is observed (Fig. 12B3), indicating that inorganic–organic modification is favorable to improve the adhesion between CSW and the PVC matrix. These results are consistent with the tensile SEM analysis.

3.6. Heat resistance

Fig. 13 shows the variation of the VST of CSW/PVC and mCSW/PVC composites as a function of CSW loading. VST could reflect the moving ability of the polymer chains, and the more difficult it is for the polymer chains to move, the higher the VST will be.[39]

of CSW from the PVC matrix because of the poor interfacial interaction; in Fig. 12A2, only few eTi$_{4000}$-CSW are pulled out from the matrix, and most of them are fractured owing to the strong interfacial adhesion between eTi$_{4000}$-CSW and the matrix, whereas in Fig. 12A3, almost all eTi$_{4000}$-OH-CSW are fractured and embedded in the PVC matrix, indicating that the inorganic–organic modification effectively improves the interfacial adhesion strength. The SEM images of the composites with 30 wt% whisker are shown in Fig. 12B1–B3. The fractured surface of CSW/PVC composite with 30 wt% whisker shows obvious agglomeration of CSW with debonding and smooth surface, which can be attributed to the poor adhesion between CSW and PVC. In Fig. 12B2, the agglomeration of CSW becomes less pronounced.

Fig. 14 TGA curves of CSW/PVC and modified CSW/PVC composites with 10 wt% whisker.

It is clear that the VST of CSW/PVC, eTi$_{4000}$-CSW/PVC and eTi$_{4000}$-OH-CSW/PVC increases with the increase of whisker loading, because whiskers can restrict the mobility of the PVC segments due to their large length-to-diameter ratio.[40] In addition, the VSTs of eTi$_{4000}$-CSW/PVC composites are higher than that of CSW/PVC composites due to enhanced interfacial adhesion. The VST of eTi$_{4000}$-OH-CSW/PVC composites are even further higher than that of eTi$_{4000}$-CSW/PVC composites at the same whisker loading due to the stronger interfacial adhesion, which could more effectively hinder the motion of PVC chains.

3.7. Thermal stability

The TGA and DTG curves of PVC, CSW/PVC, eTi$_{4000}$-CSW/PVC and eTi$_{4000}$-OH-CSW/PVC composites are shown in Fig. 14 and 15, respectively. As reported previously,[26] two weight loss stages are observed for all composites. For pure PVC, the first weight loss stage occurs at about 273 °C, which could be due to the dehydrochlorination and the formation of double bonds along the polymer chain.[41] In the temperature range of 292–426 °C, the pure PVC becomes thermally stable again because of the formation of conjugated double bonds after the removal of HCl.[42] The second decomposition stage occurs at 426–473 °C, which corresponds to the polyacetylene cracking (the scission of covalent and multiple bonds). A stable residue (i.e., carbon black) is formed at temperatures higher than 473 °C.[43]

The temperatures of onset decomposition (T_{onset}), rapidest decomposition (T_{rpd}), and 50% weight loss residue (T_{50}) are summarized in Table 4. It is shown that the T_{onset} and T_{rpd} of modified CSW/PVC composites are higher than that of CSW/PVC composites and pure PVC, indicating an improvement of thermal degradation in mCSW/PVC composites. In addition, the T_{onset} and T_{rpd} of eTi$_{4000}$-OH-CSW/PVC composites are higher than that of eTi$_{4000}$-CSW/PVC composites, because the coupling agents can improve the interface adhesion between CSW and the PVC matrix,[43,44] and OH-CSW can bond more coupling agents after hydroxylation.

Table 4 Degradation temperatures of PVC and its composites obtained from TGA curves

Samples	Temperature (°C)		
	T_{onset}	T_{rpd}	T_{50}
Pure PVC	273	280	313
CSW/PVC	275	282	331
eTi$_{4000}$-CSW/PVC	276	286	332
eTi$_{4000}$-OH-CSW/PVC	285	289	330

4. Conclusions

In this study, CSW coated with Ca(OH)$_2$ has been successfully prepared by hydroxylation modification and then further modified by eTi$_{4000}$. The results show that hydroxylation modification makes CSW more hydrophilic due to the increase of hydroxyl groups. eTi$_{4000}$-OH-CSW shows a further improvement of hydrophobicity resulting from more coupling agents bonded on the OH-CSW surface. Thus, eTi$_{4000}$-OH-CSW/PVC composites display better mechanical and thermal properties than that of CSW/PVC and eTi$_{4000}$-CSW/PVC counterparts. The yield strength and Young's modulus of the eTi$_{4000}$-OH-CSW/PVC composite with 30 wt% CSW reaches 53.8 MPa and 2319 MPa with an increase of 33.8% and 20.7% compared with CSW/PVC composite, and 24.2% and 21.3% compared with eTi$_{4000}$-CSW/PVC with the same CSW content, respectively. The flexural modulus of eTi$_{4000}$-OH-CSW/PVC composite with 15 wt% CSW is 3807 MPa, with an increase of 28.6% and 18.5% compared with CSW/PVC and eTi$_{4000}$-CSW/PVC composites with the same CSW content, respectively. In addition, eTi$_{4000}$-OH-CSW/PVC composites have better thermal stability than their CSW/PVC and eTi$_{4000}$-CSW/PVC counterparts.

Conflicts of interest

There are no conflicts to declare.

Acknowledgements

References

1 J. Cui, Y. Cai, W. Yuan, Z. Lv and S. Xu, Preparation of a Crosslinked Chitosan Coated Calcium Sulfate Whisker and Its Reinforcement in Polyvinyl Chloride, J. Mater. Sci. Technol., 2016, 32, 745–752, DOI: 10.1016/j.jmst.2016.06.006.
2 J.-Y. Cui, Y.-B. Cai, W.-J. Yuan, Z.-F. Lv, C. Zhang and S.-A. Xu, Preparation of PMMA grafted calcium carbonate whiskers and its reinforcement effect in PVC, Polym. Compos., 2015, 16, 1–9, DOI: 10.1002/pc.23873.
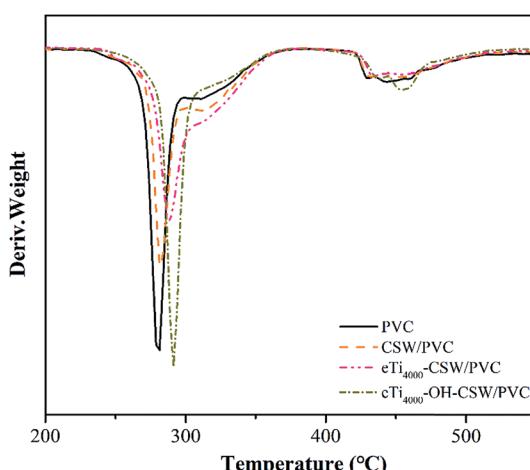
Fig. 15 DTG curves of CSW/PVC and modified CSW/PVC composites with 10 wt% whisker.

3 W. Yuan, J. Cui, Y. Cai and S. Xu, A novel surface modification for calcium sulfate whisker used for reinforcement of poly(vinyl chloride), *J. Polym. Res.*, 2015, **22**, 800, DOI: 10.1007/s10965-015-0813-4.

4 W. Yuan, J. Cui and S. Xu, Mechanical Properties and Interfacial Interaction of Modified Calcium Sulfate Whisker/Poly(Vinyl Chloride) Composites, *J. Mater. Sci. Technol.*, 2016, **32**, 1352–1360, DOI: 10.1016/j.jmst.2016.05.016.

5 W. Yuan, Y. Lu and S. Xu, Synthesis of a New Titanate Coupling Agent for the Modification of Calcium Sulfate Whisker in Poly(Vinyl Chloride) Composite, *Materials*, 2016, **9**, 625, DOI: 10.3390/ma9080625.

6 Y. Wang, Y. Li, A. Yuan, B. Yuan, X. Lei, Q. Ma, J. Han, J. Wang and J. Chen, Preparation of calcium sulfate whiskers by carbide slag through hydrothermal method, *Cryst. Res. Technol.*, 2014, **49**, 800–807, DOI: 10.1002/crat.201400155.

7 X. L. Wang, Y. M. Zhu, Y. X. Han, Z. T. Yuan and W. Z. Yin, Toughening of Polypropylene with Calcium Sulfate Whiskers Treated by Coupling Agents, *AMR*, 2009, **58**, 225–229, DOI: 10.4028/www.scientific.net/AMR.58.225.

8 H.-G. Wang, B. Mu, J.-F. Ren, L.-Q. Jian, J.-Y. Zhang and S.-R. Yang, Mechanical and tribological behaviors of PA66/PVDF blends filled with calcium sulphate whiskers, *Polym. Compos.*, 2009, **30**, 1326–1332, DOI: 10.1002/pc.20699.

9 S. Yun, Q. Song, D. Zhao, G. Qian, X. Li and W. Li, Study on the inorganic–organic surface modification of potassium titanate whisker, *Appl. Surf. Sci.*, 2012, **258**, 4444–4448, DOI: 10.1016/j.apsusc.2012.01.003.

10 C. Liu, Q. Zhao, Y. Wang, P. Shi and M. Jiang, Surface modification of calcium sulfate whisker prepared from flue gas desulfurization gypsum, *Appl. Surf. Sci.*, 2016, **360**, 263–269, DOI: 10.1016/j.apsusc.2015.11.032.

11 Q. Jiang, Y. Cheng, X.-Y. Cao, R. Wei and M. Zhao, Preparation and physical properties of chitosan-coated calcium sulphate whiskers, *Chem. Pap.*, 2014, **68**, 280, DOI: 10.2478/s11696-014-0579-x.

12 X. Feng, Y. Zhang, G. Wang, M. Miao and L. Shi, Dual-surface modification of calcium sulfate whisker with sodium hexametaphosphate/silica and use as new water-resistant reinforcing fillers in papermaking, *Powder Technol.*, 2015, **271**, 1–6, DOI: 10.1016/j.powtec.2014.11.015.

13 D. Zhu, X. Nai, S. Lan, S. Bian, X. Liu and W. Li, Surface modification of magnesium hydroxide sulfate hydrate whiskers using a silane coupling agent by dry process, *Appl. Surf. Sci.*, 2016, **390**, 25–30, DOI: 10.1016/j.apsusc.2016.08.033.

14 K. M. Praveen, S. Thomas, Y. Grohens, M. Mozetič, I. Junkar, G. Primc and M. Gorjanc, Investigations of plasma induced effects on the surface properties of lignocellulosic natural coir fibres, *Appl. Surf. Sci.*, 2016, **368**, 146–156, DOI: 10.1016/j.apsusc.2016.01.159.

15 J.-H. Lee, P. Zapata, S. Choi and J. C. Meredith, Effect of nanowhisker-modified zeolites on mechanical and thermal properties of poly(vinyl acetate) composites with pure-silica

MFI, *Polymer*, 2010, **51**, 5744–5755, DOI: 10.1016/j.polymer.2010.09.071.

16 L. Dang, X. Nai, D. Zhu, Y. Jing, X. Liu, Y. Dong and W. Li, Study on the mechanism of surface modification of magnesium oxysulfate whisker, *Appl. Surf. Sci.*, 2014, **317**, 325–331, DOI: 10.1016/j.apsusc.2014.07.205.

17 J. Prachayawarakorn, S. Khunsumled, C. Thongpin, A. Kositchaiyong and N. Sombatsompop, Effects of silane and MAPE coupling agents on the properties and interfacial adhesion of wood-filled PVC/LDPE blend, *J. Appl. Polym. Sci.*, 2008, **108**, 3523–3530, DOI: 10.1002/app.27973.

18 B. K. Deka and T. K. Maji, Effect of coupling agent and nanoclay on properties of HDPE, LDPE, PP, PVC blend and Phargamites karka nanocomposite, *Compos. Sci. Technol.*, 2010, **70**, 1755–1761, DOI: 10.1016/j.compscitech.2010.07.010.

19 M. Abdelmouleh, S. Boufi, M. Belgacem and A. Dufresne, Short natural-fibre reinforced polyethylene and natural rubber composites, *Compos. Sci. Technol.*, 2007, **67**, 1627–1639, DOI: 10.1016/j.compscitech.2006.07.003.

20 L. M. Matuana, R. T. Woodhams, J. J. Balatinecz and C. B. Park, Influence of interfacial interactions on the properties of PVC/cellulosic fiber composites, *Polym. Compos.*, 1998, **19**, 446–455, DOI: 10.1002/pc.10119.

21 Y. Nakamura, A. Harada, T. Gotoh, N. Yokouchi and T. Iida, Effect of silane chain length on the mechanical properties of silane-treated glass beads-filled PVC, *Compos. Interfaces*, 2012, **14**, 117–130, DOI: 10.1163/156855407779819035.

22 S.-r. Ma, L.-y. Shi, X. Feng, W.-j. Yu and B. Lu, Graft modification of ZnO nanoparticles with silane coupling agent KH570 in mixed solvent, *J. Shanghai Univ.*, 2008, **12**, 278–282, DOI: 10.1007/s11741-008-0316-1.

23 T. Le Truong, Å. Larsen, B. Holme, S. Diplas, F. K. Hansen, J. Roots and S. Jørgensen, Dispersibility of silane-functionalized alumina nanoparticles in syndiotactic polypropylene, *Surf. Interface Anal.*, 2010, **42**, 1046–1049, DOI: 10.1002/sia.3166.

24 L. Yang, Y. Hu, H. Guo, L. Song, Z. Chen and W. Fan, Toughening and reinforcement of rigid PVC with silicone rubber/nano-CACO$_3$ shell–core structured fillers, *J. Appl. Polym. Sci.*, 2006, **102**, 2560–2567, DOI: 10.1002/app.24685.

25 B. L. Shah, L. M. Matuana and P. A. Heiden, Novel coupling agents for PVC/wood-flour composites, *J. Vinyl Addit. Technol.*, 2005, **11**, 160–165, DOI: 10.1002/vnl.20056.

26 Y. Lu, W. Zhang, X. Li and S. Xu, Synthesis of new polyether titanate coupling agents with different polyethyleneglycol segment lengths and their compatibilization in calcium sulfate whisker/poly(vinyl chloride) composites, *RSC Adv.*, 2017, **7**, 31628–31640, DOI: 10.1039/c7ra03692b.

27 S. Chen, Q. Wang and T. Wang, Mechanical, damping, and thermal properties of calcium sulfate whisker-filled castor oil-based polyurethane/epoxy IPN composites, *J. Reinf. Plast. Compos.*, 2011, **30**, 509–515, DOI: 10.1177/0731684411398539.

28 B. Lauke, Plastic yielding contribution to fracture toughness of polymers modified with rubber and inorganic fillers, *J.*

Mater. Sci., 2015, **50**, 2178–2188, DOI: 10.1007/s10853-014-8781-3.

29 F. N. Ahmad, M. Jaafar, S. Palaniandy and K. A. M. Azizli, Effect of particle shape of silica mineral on the properties of epoxy composites, *Compos. Sci. Technol.*, 2008, **68**, 346–353, DOI: 10.1016/j.compscitech.2007.07.015.

30 D. Metın, F. Tihminlioğlu, D. Balköse and S. Ülkü, The effect of interfacial interactions on the mechanical properties of polypropylene/natural zeolite composites, *Composites, Part A*, 2004, **35**, 23–32, DOI: 10.1016/j.compositesa.2003.09.021.

31 G. M. G.-M. Kim, Micromechanical deformation processes in toughened and particle filled semicrystalline polymers. Part 2: Model representation for micromechanical deformation processes, *Polymer*, 1998, **39**, 5699–5703.

32 A. Dufresne, Dynamic mechanical analysis of the interphase in bacterial polyester/cellulose whiskers natural composites, *Compos. Interfaces*, 2012, **7**, 53–67, DOI: 10.1163/156855400300183588.

33 G. Gilli and P. Gilli, Towards an unified hydrogen-bond theory, *J. Mol. Struct.*, 2000, **552**, 1–15, DOI: 10.1016/S0022-2860(00)00454-3.

34 I. Rozas, I. Alkorta and J. Elguero, Behavior of Ylides Containing N, O, and C Atoms as Hydrogen Bond Acceptors, *J. Am. Chem. Soc.*, 2000, **122**, 11154–11161, DOI: 10.1021/ja0017864.

35 V. Kovacevic, S. Lucic, D. Hace and A. Glasnovic, Rheology and morphology of poly(vinyl acetate) + calcite films, *Polym. Eng. Sci.*, 1996, **36**, 1134–1139, DOI: 10.1002/pen.10507.

36 O. Yuehun, Y. Feng, Z. Yan and Q. Zongneng, Study of the polymethylmethacrylate/SiO$_2$ nano-composites by *in situ* polymerization, *Acta Polym. Sin.*, 1997, **1**, 199–204.

37 S. C. Tjong, S.-A. Xu, R. K.-Y. Li and Y.-W. Mai, Short glass fiber-reinforced polyamide 6,6 composites toughened with maleated SEBS, *Compos. Sci. Technol.*, 2002, **22**, 2017–2027.

38 S. C. Tjong, S.-A. Xu and Y. W. Mai, Drop weight impact and work of fracture of short glass fiber reinforced polypropylene composites toughened with elastomer, *Polym. Compos.*, 2003, **24**, 437–447.

39 L. Yang, D. Sun, Y. Li, G. Liu and J. Gao, Properties of poly(vinyl chloride) blended with an emulsion copolymer of *N*-cyclohexylmaleimide and methyl methacrylate, *J. Appl. Polym. Sci.*, 2003, **88**, 201–205, DOI: 10.1002/app.11646.

40 T. Yu, Y. Li and J. Ren, Preparation and properties of short natural fiber reinforced poly(lactic acid) composites, *Trans. Nonferrous Met. Soc. China*, 2009, **19**, s651–s655, DOI: 10.1016/S1003-6326(10)60126-4.

41 H. Djidjelli, T. Sadoun and D. Benachour, Effect of plasticizer nature and content on the PVC stability and dielectric properties, *J. Appl. Polym. Sci.*, 2000, **78**, 685–691, DOI: 10.1002/1097-4628(20001017)78:3<685::AID-APP250>3.0.CO;2-F.

42 R. Benavides, B. M. Castillo, A. O. Castañeda, G. M. López and G. Arias, Different thermo-oxidative degradation routes in poly(vinyl chloride), *Polym. Degrad. Stab.*, 2001, **73**, 417–423, DOI: 10.1016/S0141-3910(01)00122-7.

43 I. K. Bishay, S. L. Abd-El-Messieh and S. H. Mansour, Electrical, mechanical and thermal properties of polyvinyl chloride composites filled with aluminum powder, *Mater. Des.*, 2011, **32**, 62–68, DOI: 10.1016/j.matdes.2010.06.035.

44 X. Li, B. Lei, Z. Lin, L. Huang, S. Tan and X. Cai, The utilization of bamboo charcoal enhances wood plastic composites with excellent mechanical and thermal properties, *Mater. Des.*, 2014, **53**, 419–424, DOI: 10.1016/j.matdes.2013.07.028.